ARTICLE

Synthesis, post-synthetic modification and stability of 2D styrylammonium lead iodide hybrid material

Received 00th January 20xx,
Accepted 00th January 20xx

DOI: 10.1039/x0xx00000x

Yong Peng,[a] Josep Albero*[a] and Hermenegildo Garcia*[c]

A new hybrid lead iodide material (HP1) having 4-vinylphenylene ammonium as organic cation has been prepared. The structural formula based on chemical analysis for HP1 corresponds to $PbI_{2.5}$(4-styrylammonium)$_{0.5}$. The crystallinity of HP1 was confirmed by powder X-ray diffraction and high resolution transmission electron microscopy. The presence of the styryl ammonium moiety in HP1 allows post-synthetic modification by radical copolymerization with styrene to obtain material HP2 with higher hydrophobicity. Stability tests show that both HP1 and HP2 undergo in the dark hydrogen evolution, indicating partial decomposition of the hybrid material in a percentage of about 0.6 %. This hydrogen evolution increases by a factor of 3 when HP1 and HP2 are exposed to visible light. X-ray photoelectron spectroscopy analysis shows an increase of NH_2 groups and a decrease of NH_3^+ units suggesting that the origin of hydrogen evolution is deprotonation of ammonium ions.

Introduction

The excellent optoelectronic properties of lead halide hybrid perovskites, particularly, methylammonium perovskites have revolutionized the field of photovoltaics.[1-5] Hybrid lead perovskites and related materials can absorb a considerable percentage of the solar radiation and due to the low exciton binding energy and high charge carrier mobility, exhibit high charge separation efficiency.[6-9] In comparison, with the slow pace in the increase of photovoltaic efficiency that has characterized dye sensitized solar cells, hybrid perovskites solar cells have reached an impressive 25.2 % efficiency in just a few years after the initial discovery of their photovoltaic properties.[10-12]

The mechanism of operation of photovoltaic cells has many common elementary steps with photocatalysis, including light harvesting, charge separation and charge migration to the particle surface, being the main difference the occurrence of surface redox reactions, transforming substrates on the particles, in the case of photocatalysis, compared to interparticle charge migration in photovoltaic devices.[13-14] However, in contrast to the importance of hybrid lead perovskites in photovoltaics, these hybrid materials have been almost ignored as photocatalysts, the main reason for this being the notorious lack of stability of these materials under ambient conditions, particularly, when exposed to humidity.[15-17] It has been widely reported that contacting these materials with the ambient moisture results in strong water adsorption that eventually has been proposed to replace I^- ions by hydroxyl groups.[18-19] Therefore, new approaches to avoid water adsorption in hybrid lead halide materials are very convenient to improve their stability under ambient conditions not only in the photovoltaic field, but also for their use as photocatalysts. Since hybrid perovskites allow the possibility to use different organic cations, it occurred to us that it could be possible to take advantage of organic reactions to modify their surface at will.[14, 20-23] The properties of the obtained materials could change in such a way that they could present striking properties from the photocatalytic point of view.

In that context, in contrast to the three-dimensional (3D) structure of PbI_3MA, it has been found that accommodation of larger organic ammonia ions results in a change from 3D structure to materials with lower dimensionality. More specifically, the synthesis of hybrid lead perovskites containing benzyl ammonium cation exhibit a 2D structure that allows to accommodate the benzyl side chains within the interlayer space.[24-26] These two dimensional structures have shown larger hydrophobicity and, therefore, improved photo, thermal and moisture stability.[27] In the present work, we report the synthesis of a new 2D hybrid material having styryl ammonium as organic cation, lead as inorganic cation and iodide anions. The interest of this organic unit is that the presence of the styryl units would allow subsequent further modification by radical polymerization under conditions compatible with the stability of the hybrid material. The data that will be presented here shows the

[a] *Instituto Universitario de Tecnología Química CSIC-UPV, Universitat Politècnica de València, Avda. De los Naranjos s/n 46022, Valencia (Spain). E-mails: joalsan6@itq.upv.es and hgarcia@qim.upv.es ; Tel. +34 963877807.*

† Footnotes relating to the title and/or authors should appear here.
Electronic Supplementary Information (ESI) available: [details of any supplementary information available should be included here]. See DOI: 10.1039/x0xx00000x

feasibility of this approach that could be used for post-synthetic modification of hybrid perovskites and related materials.

Experimental section

Materials

MilliQ water was obtained using an IQ 7000 purifying system. Ethanol absolute (analytical grade), tetrahydrofuran anhydrous 99.99 % (THF), diethyl ether (puriss. p.a. ACS reagent dried 0.05 % GC 0.0075 % water) and hexane (HPLC grade) were purchased from Scharlau. 4-Vinylaniline (97%), tetradecane (≥ 99 %), aqueous hydriodic acid (HI, 55 wt%), lead iodide (99.999 % trace metals basis, PbI_2), benzoyl peroxide (75%), lead bromide (99.999 % trace metals basis, $PbBr_2$), potassium iodide (99.5%, KI) and deuterium oxide (D_2O) were purchased from Sigma Aldrich. All solvents and reagents were used without further purification.

Synthesis method

Preparation of 4-styryl ammonium. Styryl ammonium was obtained by protonation of the amino group. To avoid polymerization of the double bond during the protonation process, acetone/dry ice bath was applied. Typically, 1 g 4-aminostyrene was added to 20 mL THF under stirring and the insoluble impurities was removed by filtration. Then, 1.35 mL of concentrated hydriodic acid was added dropwise to the solution. The ammonium salt was precipitated by adding diethyl ether after 2 h reaction under acetone/dry ice cooling bath, and then washed with 400 mL of cold diethyl ether. The product was characterized by IR and NMR spectroscopy after drying under vacuum overnight.

Preparation of hybrid material 1 (HP1). 230.5 mg (0.5 mmol) PbI_2 was added to 1 mL concentrated hydriodic acid aqueous solution (55 wt%) under stirring until all the solid dissolved, then 1 mL 4-styryl ammonium aqueous solution (0.5 M) was added to the above solution dropwise. The immediately precipitated perovskite was washed with diethyl ether and dried under vacuum for overnight.

Post-synthetic of hybrid material 2 (HP2). HP2 was obtained by radical-assisted copolymerization with extra addition of styrene. Specifically, HP1 (100 mg) was dispersed in 20 mL hexane, followed by adding 2×10^{-6} M of benzoyl peroxide and 0.02 mmol of styrene. After 5 h of reaction at 50°C under argon atmosphere, the resulting HP2 was washed with diethyl ether and dried under vacuum overnight.

Characterization

Powder X-ray diffraction (XRD) patterns were collected with a Shimadzu XRD-7000 diffractometer by using Cu κ_α radiation (λ=1.5418 Å), operating at 40 kV and 40 mA at a scanning speed of 10 ° per min in the 2–90° 2θ range. Diffuse reflectance UV/Vis spectra (DRS) in the range of 200 - 800 nm were collected with a Varian Cary 5000 spectrophotometer. SEM images were acquired with a JEOL JSM 6300 apparatus equipped with an X-MAX detector of OXFORD INSTRUMENTS. Transmission electron microscopy (TEM) images were made with a Philips CM300 FEG microscope operating at 200 kV. Fourier transformed infrared (FTIR) spectra were recorded in the 4000 to 400 cm^{-1} range using a Thermo Nicolet 6700 FTIR with ATR accessory instrument (Thermo scientific, USA). Lead and iodine content in HP1 were determined by using X-ray fluorescence spectroscopy (Philips MiniPal 25 fm) and a mechanical mixture of $PbBr_2$ and KI powders as calibration standards. X-ray photoelectron spectra (XPS) were measured on a SPECS spectrometer equipped with a Phoibos 1509MCD detector using a nonmonochromatic X-ray source (Al and Mg) operating at 200 W. The samples were evacuated in the prechamber of the spectrometer at 1×10^{-9} mbar. The measured intensity ratio of the components was obtained from the area of the corresponding peaks after nonlinear Shirley-type background subtraction and corrected by the transition function of the spectrometer. The work function of the apparatus was calibrated with Ag, Au and Cu with a value 4.2440 eV. Combustion elemental analyses were measured on an Euro EA Elemental Analyser Eurovector. ^{1}H NMR spectra were acquired in a Bruker AV300 (300 MHz) spectrometer, Chemical shifts of ^{1}H signals are reported in ppm using the solvent peak as internal standard. Data are reported as follows: chemical shift, multiplicity (s = singlet, br = broad, d = doublet, t = triplet, sept = septuplet, m = multiplet), integral, coupling constants (Hz) and assignment.

HP1 and PH2 stability tests

Evaluation of light and oxygen stability of HP1 and HP2 was conducted by measuring the evolution of hydrogen evolution over the time. The photoreactor is a cubic aluminium sealed reactor (total volume 100 mL) with a quartz cover allowing light passthrough and independent inlet/outlet valves with a manometer to determine pressure were adapted. 20 mg of perovskites were first placed in the reactor. Then the system was purged with argon or filled with a certain amount of oxygen until reaching a final pressure of 1.3 atmosphere. A Hamamatsu Xenon lamp (235 - 850 nm) with a focused intensity on the flask of 1.3 kW/m^2 was used as a UV-vis light source. A UV cut-off filter (> 400 nm) was employed to carry out the experiments with UV filtered light.

A 0.25 mL sample of the generated gas was collected periodically with an air-tight syringe and the hydrogen content analysed by gas chromatography (GS-MOL 15 m column ID 0.55 mm TCD from J&W Scientific). All glassware was clean and carefully rinsed with Milli-Q water prior to use.

Results and discussion

Synthetic procedures

The synthesis of 4-styryl ammonium lead iodide material is illustrated in **Scheme 1**. This synthesis starts with the protonation of commercially available 4-aminostyrene by HI acid. This protonation has to be carried out carefully at low temperature (gry ice/acetone ice bath, ~ -70 °C) to avoid the occurrence of double bond polymerization and/or electrophilic additions to the C-C.[28] Protonation of the amino group results in ^{1}H NMR spectroscopy in a remarkable downfield shift of the aromatic protons at the ortho position of the amino group of about 1 ppm as well

as other changes in the chemical shifts of the protons. **Figure S1** in supporting information shows a comparison of the ^{1}H NMR spectra for 4-aminostyrene and styryl ammonium (ammonium **1**). Importantly, spectroscopic data confirm that under optimized protonation conditions, the vinylic CH=CH$_2$ group remains unaltered. IR spectroscopy also shows significant changes upon protonation, the most remarkable one being the change in the position and intensity of the NH stretch vibration bands that become more intense and shifted towards smaller wavenumber upon protonation (**Figure S2** in supporting information). The hybrid styrene-ammonium lead iodide was finally obtained by mixing a solution of PbI$_2$ in aqueous HI and ammonium salt **1**. Upon mixing, instantaneous precipitation of the hybrid material HP1 is observed. HP1 was separated by filtration and washed with diethyl ether.

Material characterization

Power XRD of HP1 is presented in **Figure 1a**, where comparison with the XRD patterns of the two components, i.e., PbI$_2$ and ammonium 1 is presented. As can be seen there, HP1 is a crystalline material with a structure different than PbI$_2$ or ammonium 1. The HP1 XRD pattern confirms that the precipitated crystals correspond to a new material, which diffraction pattern cannot be attributed to the parent` patters addition. Unfortunately, all the attempts to determine the crystal structure of HP1 by single-crystal XRD analysis were unsuccessful. However, the formation of a hybrid structure, exhibiting high crystallinity, can be elucidated from the HP1 pattern since small angle peaks bellow 10 º corresponds to the organic counterpart, while the 25 and 40 º peaks can be attributed to the inorganic Pb-I structure. Similar diffraction pattern has been reported for a mixed 2D hybrid perovskite based on methyl and polyethileneimide ammonium cations.[29] In this, a strong peak at 8 º, indicative of a 2D hybrid structure can be observed, very similar to the one observed in the present case.

FTIR of HP1 (Figure 1b) shows stretch vibration bands appearing at 3500 and from 3200 to 2500 cm^{-1} corresponding to OH and NH vibrations, respectively. The IR spectrum shows also in the aromatic region, the expected peaks from 1620 to 1450 cm^{-1}.

Interestingly, in the finger print region, the presence of an intense peak at about 800 cm^{-1} due to the para aromatic substitution of the benzyl ring and two out of plane vibration bands of vinylic groups at 980 and 915 cm^{-1} were also recorded. Particularly, the last characteristic vibration peaks indicate that the vinylic double bond CH=CH$_2$ groups are still present in the structure of HP1.

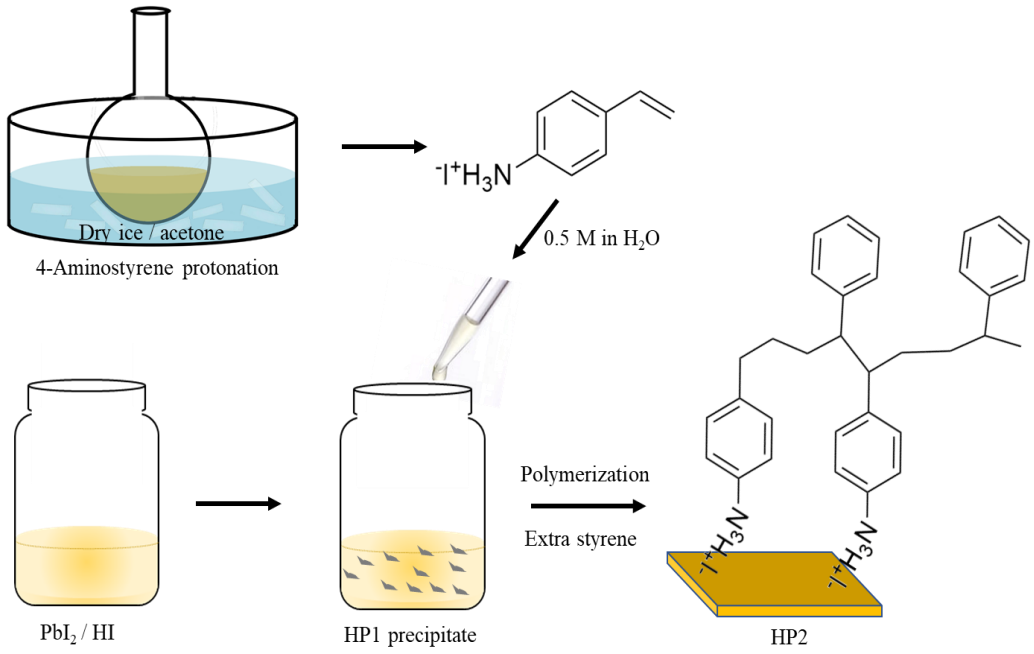

Scheme 1. Illustration of the synthesis route of HP1 and HP2.

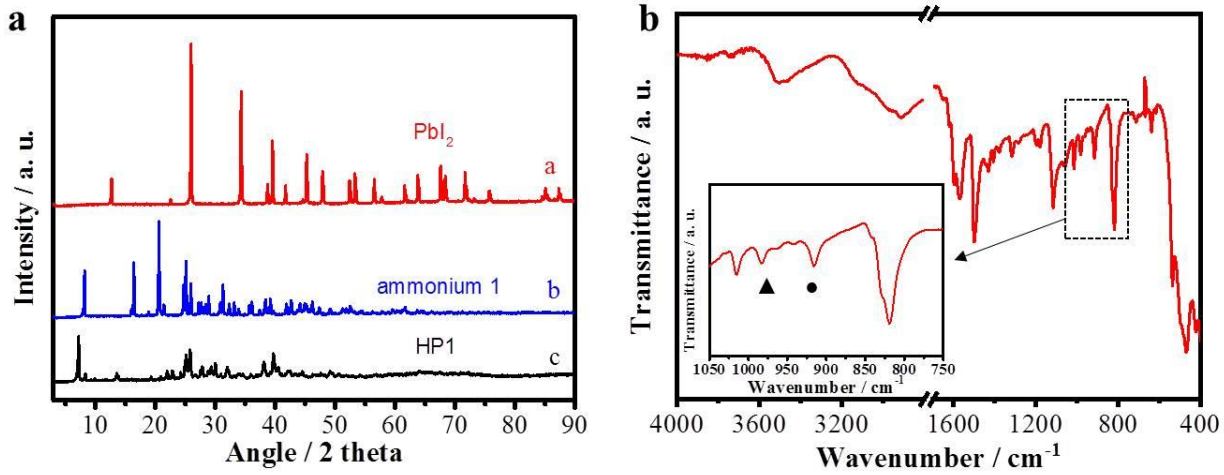

Figure 1. (a) XRD patterns of HP1 (black line), ammonium 1 (blue line) and PbI_2 (red line). (b) FT-IR spectrum of HP1. Inset: enlarged view of the black frame. ▲Out of plane bending of the –CH=, ● out of plane vibration (wagging) of the CH_2

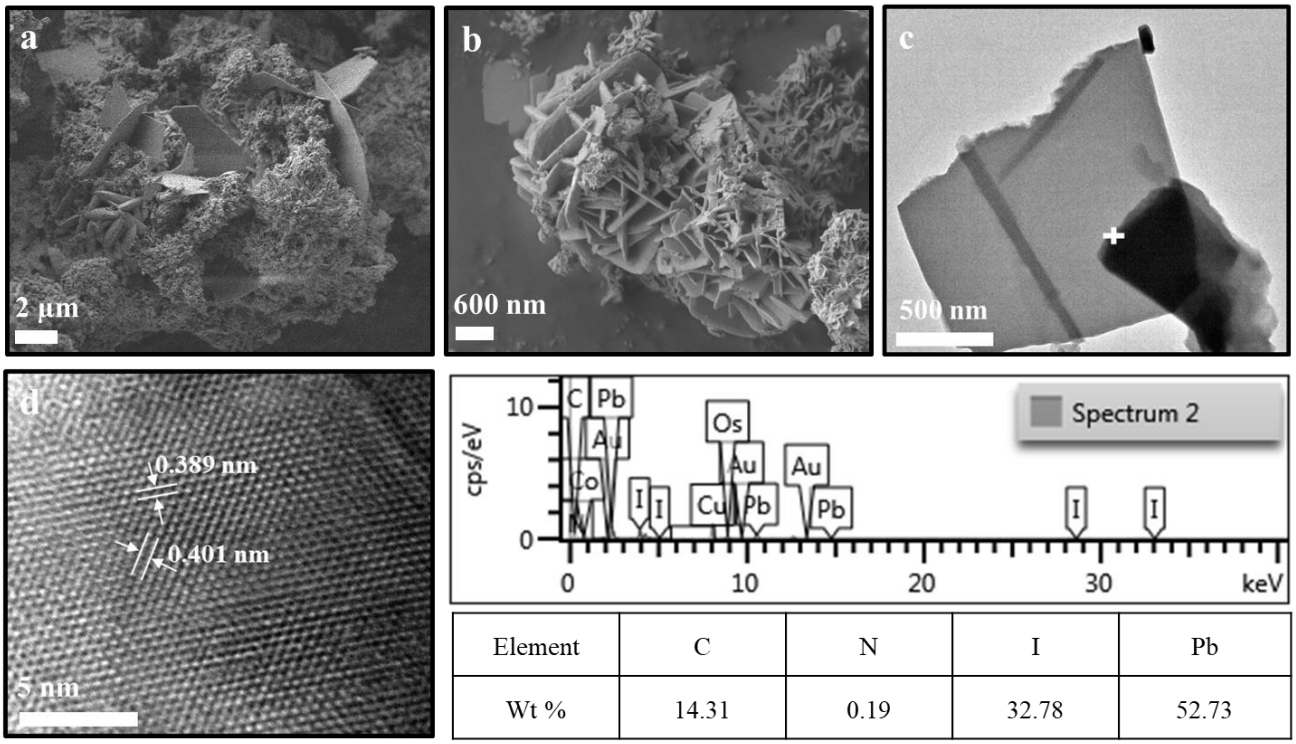

Element	C	N	I	Pb
Wt %	14.31	0.19	32.78	52.73

Figure 2. Representative images of the morphology and structure of HP1 particles obtained from SEM (a,b) and HRTEM (c,d). Panels at the bottom show the EDS analysis of HP1. Panel d shows the lattice fringes of two planes in HP1 crystal.

The morphology and composition of HP1 particles was observed by scanning electron microscopy (SEM) and high-resolution transmission electron microscopy (HRTEM) accompanied with EDS analysis, which are presented in **Figure 2**. It was observed that the material is constituted by large aggregates of about 6 μm or larger size constituted by the assembly of thin platelets. This morphology has been reported for 2D hybrid materials,[30] and suggests that also in the present case, HP1 could have such 2D dimensionality in its structure. TEM shows that HP1 is constituted by aggregation of thin platelets with dimensions larger than 500 nm up to several micrometers. High resolution images show the presence of crystalline planes of 0.389 nm and 0.401 nm that coincide with the position of two peaks in XRD pattern (2θ=22.823° and 21.975°, respectively). Overall, the high resolution TEM images confirm the high crystallinity in accordance with powder XRD and the 2D structure of the material. EDS analysis of selected area corresponding to the surface of the particle show the presence of Pb, I and C, in a relative proportion of 53, 33 and 14%, respectively, indicating that the material is constituted by these elements.

The elemental composition of HP1 was determined by combining X-ray fluorescence analysis for Pb and I, with combustion elemental analysis for C and H. The results are

presented in the supporting information (see **Table S1**). These analyses have allowed to estimate for HP1 a composition of $PbI_{2.5}1_{0.5}$. This composition does not agree with the expected formula for 3D, 2D or 1D hybrid lead perovskites that are PbI_3X,[31-32] PbI_4X_2,[33-34] and PbI_3X (facet-sharing),[35-36] respectively (in which X represents the organic ammonium cation). It could be that the defects on the structure are responsible for the deviation of the empirical formula from the ideal composition expected for these 2D materials. In this regard, it has to be commented that EDS analysis by electron microscopy shows that the surface of HP1 is enriched of Pb and has a low average content of I. The presence of O on HP1 surface is also detectable by EDS**.**

Analytic data of HP1 by XRF and combustion elemental analysis or EDS was complemented by XPS. Survey XPS analysis detected the expected elements according to the empirical formula plus the presence of oxygen. High resolution peaks for C1s, N1s, O1s, Pb4f and I3d are shown in **Figure 3**. C1s, Pb4f and I3d are mainly composed by a single component, corresponding to sp2 carbons, Pb^{2+} and I^-, respectively.[37] In contrast, N1s peak shows two components at 399.5 and 402.5 in a proportion of 44 and 56 %, attributable to $-NH_2$ and $-NH_3^+$.[38] This distribution of N atoms could indicate that styryl ammonium ligand is deprotonated in a significant proportion. This is compatible with the fact that XPS analysis also detects the presence of oxygen atoms in the outermost part of the particles. The deconvolution of the high resolution O1s peak indicates that there are three main components at 529.0 (25 %), 532.0 (39 %), and 533.5 eV (36 %), that can be attributed to Pb-O, Pb-OH and adsorbed H_2O, respectively.[39] According to this analysis, part of the positive charges on the external surface of the HP1, resulted from the exposed Pb^{2+}, should be compensated by hydroxyl and oxide groups.

XPS also allows to determine the energy of the valence band edge by extrapolating the first electron emission peak at lower energy (see the description of the calculation in the supporting information). According to this measurement, the valence band energy of the hybrid material HP1 was determined at -5.34 eV referred to vacuum. The HP1 optical bandgap, assuming that the obtained material presents a direct bandgap, was estimated by the Tauc plot (Figure S3), and was determined of 2.63 eV. It is worth noticing that an small band can be distinguished in the Tauc plot at lower energy. We have attributed this band to mid-gap states created as consequence of structural defects. The energy gap of this transition was determined to 2.42 eV. The band gap value together with the valence band position allow us to calculate the energy of the conduction band energy, which is about - 2.71 eV. The diffuse reflectance spectrum from which the optical bandgap was estimated is presented in **Figure S3** in supplementary information. As it can be seen there, the absorption band presents a shoulder of the main absorption band at 490 nm, attributed to mid-gap states and it have relative maximums at 425, 400 and 310 nm, which can be attributed to excitonic peaks related with the 2D morphology. This absorption spectrum corresponding to HP1 is different from the styryl ammonium iodide that has a weak absorption band at 360 nm and an intense absorption at 290 nm. The absorption spectrum of HP1 is also different from that of PbI_2 that has a very step absorption at 550 nm.

It is worth commenting that the obtained HP1 UV-Vis spectrum presents different characteristics than that of the overlap of the parent precursors UV-Vis spectra, indicating that HP1 cannot be a mixture of PbI_2 and the organic precursor.

Post-synthetic modification

After HP1 characterization, post-synthetic modification was performed by carrying out radical polymerization of the styryl moieties with additional amount of styrene. As commented in the introduction, the leading idea of the present work was the preparation of a semiconductor material with an organic ligand that allows surface modification by an organic reaction under mild conditions. Styryl ammonium was selected with this purpose since it was considered that the styryl moiety of the ammonium ligand should allow copolymerization with styrene molecules. The key point is to find a reaction compatible with the structural stability of the hybrid material. In this sense, styrene polymerization initiated by radicals can be carried out under inert atmosphere at moderate temperature (50 ^oC), and in non-polar organic solvent (hexane). This post-synthetic modification of HP1 allows us the control of the properties of the particle surface without altering the optoelectronic properties of the hybrid material.

The success of the polymerization was confirmed by FTIR and NMR spectroscopy. On the contrary, the crystallinity and optoelectronic properties of HP1 were preserved after this post-synthetic modification, as can be observed by XRD and diffuse reflectance UV-Vis spectroscopy in Figures S4 and S5, respectively, in supplementary information. As can be observed in these Figures, the crystallinity, phase and optoelectronic properties of HP1 have been preserved after polymerization, indicating that the HP1 material has not suffered any change under these reaction conditions. FTIR spectroscopy reveals the disappearance of the characteristic out of plane vibration bands corresponding to the vinylic moiety (915 and 980 cm^{-1}), which indicates the occurrence of double bond polymerization of styryl ammonium (see Figure 4).

ARTICLE

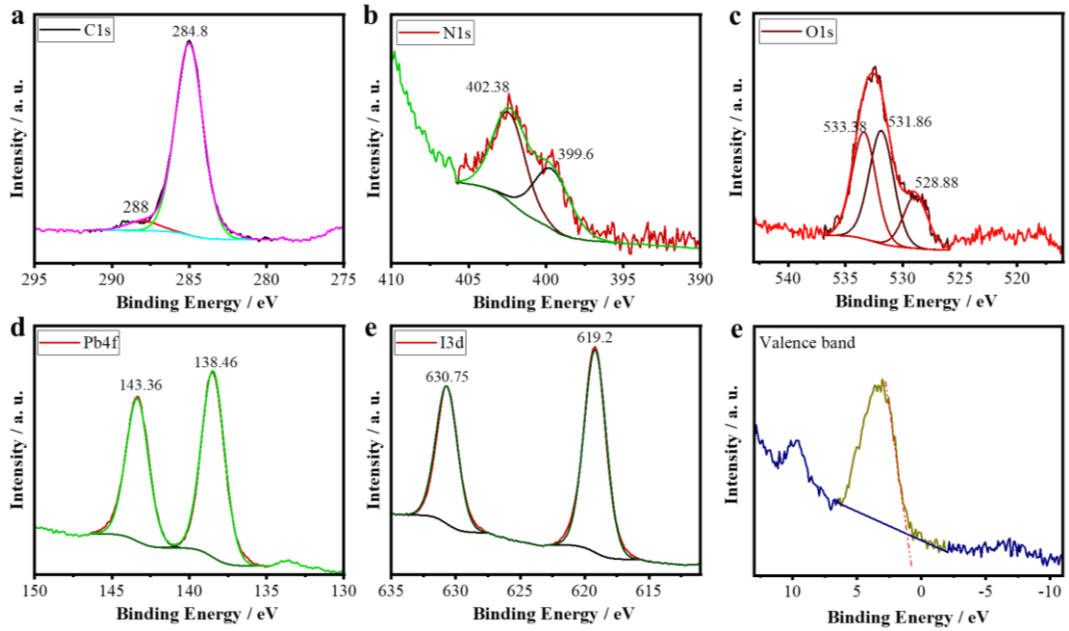

Figure 3. High resolution XPS C1s (a), N1s (b), O1s (c), Pb 4f (d) and I 3d (e) peaks. Valence band edge determined from the first electron band in XPS (e).

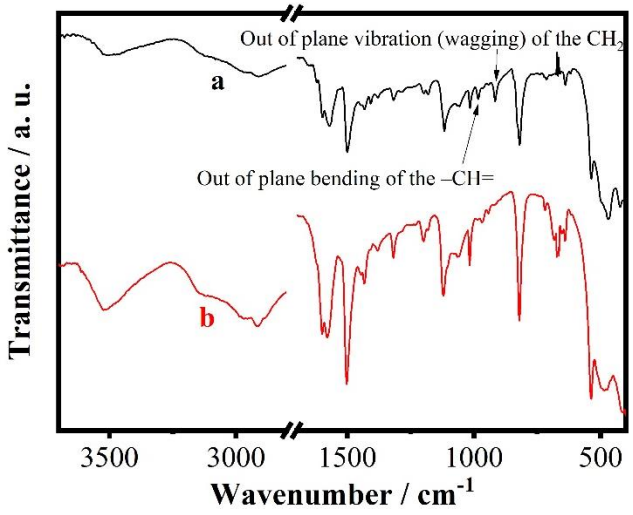

Figure 4. FTIR spectroscopy of HP1 (a) and HP2 (b). The disappearance of peaks at 980 and 915 cm^{-1} indicates the occurrence of double bond polymerization of ammonium styrene.

To obtain additional evidence of the occurrence of polymerization involving the styryl units, samples of HP1 and HP2 were dispersed in deuterated D_2O and the obtained liquid supernatants, containing organic ammonium moieties extracted from HP1 or HP2, were analyzed by ^1H NMR spectroscopy. The results are presented in **Figure S6** in the supporting information. As can be seen there, in the case of HP1, the ^1H NMR spectrum corresponding to styryl ammonium ligand was recorded. Specifically, signals corresponding to the three vinylic hydrogens appearing at 6.75 (d-d, 1H, J^3=10.59 Hz and J^3=17.94 Hz), 5.0 (d-d, 1H, J^3=17.94 Hz) and 5.35 (d-d, 1H, J^3= 10.59 Hz), were recorded. In contrast, similar experiment for HP2 exhibits a barely detectable signal for these vinyl protons and the more complex aromatic region was accompanying by aliphatic signals indicating the success of polymer formation.

Copolymerization of HP1 with styrene results in clear morphologic change of the HP2 particles respect to the parent HP1 material. Some representative images are provided in the supporting information (**Figure S7**). As can be seen there, copolymerization results in the formation of smooth surfaces in SEM images reflecting the coating of the original flower-like particle by polystyrene.

As it could be expected, considering the hydrophobic properties of polystyrene, HP2 exhibits a remarkable hydrophobicity that is visually observed by HP2 floating in water. Nevertheless, as commented before, HP2 becomes eventually decomposed upon stirring. In contrast, HP1 undergoes instantaneously decomposition under the same conditions. **Figure S8** shows some photographs to illustrate the distinctive behaviour of HP1 and HP2 in water.

Photostability tests

As also commented in the introduction, the long-term goal of this research is the development of hybrid materials that could be used as photocatalyst, exhibiting photostability. For this reason, it was of interest to determine the relative stability of HP1 and HP2, both in the dark, and, under illumination (λ > 400 nm). It was observed that upon standing at room temperature in the absence and presence of oxygen, H_2 evolution occurs for both HP1 and HP2 in the dark. This hydrogen evolution increases in HP1 and HP2 samples upon visible light irradiation in the absence of oxygen, but H_2 evolution significantly enhance when HP1 and HP2 are irradiated in the presence of oxygen. **Figure 5** shows the temporal H_2 evolution for the two samples under the conditions tested. As can be seen there, the differences in the H_2 evolution for HP1 and HP2 are very minor, indicating that coating of the particles by polystyrene does not alter the stability of the hybrid perovskite against light or oxygen. Quantification of the amount of hydrogen evolved indicates, however, that it corresponds to a minor percentage of the estimated amount of the total organic ligand in the material. Overall, the detection of hydrogen in these samples indicates that they are instable, although the amount of hydrogen corresponds to a minor percentage of the decomposition.

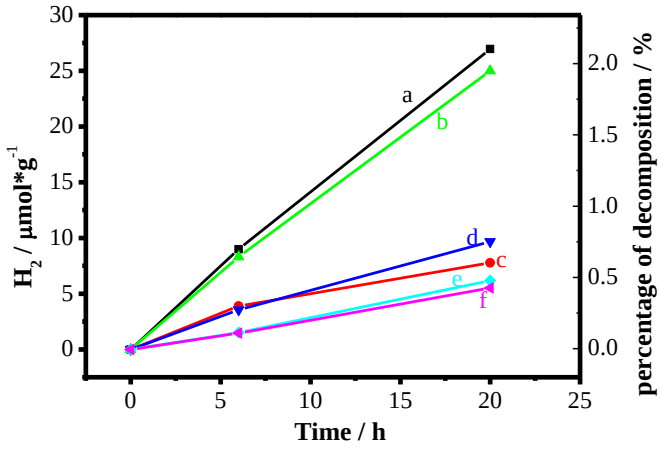

Figure 5. Hydrogen evolution under different conditions: (a, black squares) HP1 under light and O_2, (b, green triangles) HP2 under light and O_2, (c, red dots) HP2 under light and Ar, (d, blue inverse triangles) HP1 under light and Ar, (e, cyan diamonds) HP1 under dark and O_2, and (f, pink triangles) HP2 under dark and O_2.

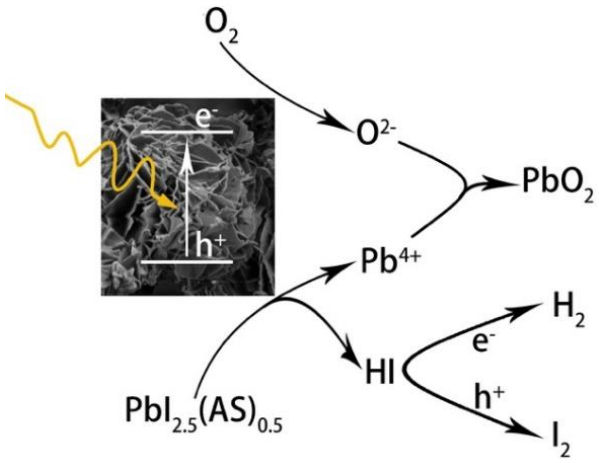

Scheme 2. Proposed mechanism of HP1 and HP2 decomposition and pathways of resulting in H_2 evolution.

It is proposed that hydrogen formation is a secondary process that derives from the initial formation of HI. It has been proposed that evolution of HI is the main cause of decomposition of methyl ammonium perovskite and the same could happen in the present case.[40-41] From HI, hydrogen will be formed by splitting and the process could be assisted by the presence of oxygen. **Scheme 2** illustrates the proposed pathways resulting in hydrogen evolution. This mechanism involves the photogeneration of e^-/h^+ pairs first. Then, e^- are efficiently quenched in the presence of oxygen, generating superoxide radicals (O^{2-}). The photogenerated h^+ promote Pb oxidation to Pb^{4+}, which in the presence of O^{2-} promotes PbO_2. The later oxidation induces HI evolution, and, in the presence of e^-/h^+ pairs, I_2 and H_2 are eventually produced. It appears that surface modification does not influence this decomposition mechanism and the behaviour of HP1 and HP2 is similar.

In support of the proposal to explain hydrogen evolution from hybrid perovskite, XPS analysis of the samples after light irradiation shows an increase of the percentage of NH_2 with respect to NH_3^+ in the high resolution N1s peak of the irradiated sample showing that the deprotonation has occurred. Also, analysis of the Pb4f peak shows the appearance of a component of 15 % corresponding to Pb^{4+} in the sample. These changes were also detectable after HP1 sample was submitted to light irradiation in the absence of O_2 (**Figure S9**).

Conclusions

The present study has shown the preparation of a new 2D hybrid lead halide material and its post-synthetic modification based on the organic reaction of the ammonium ligand. This strategy has been illustrated in the present case by the synthesis of a new hybrid lead halide material with styryl ammonium ligand that, after the synthesis, is submitted to cross-polymerization with styrene. Although spectroscopic evidences confirm the success of the cross polymerization with subsequent increase in the hydrophobicity of the modified hybrid perovskite, the stability of this material in water is still not sufficient and can become dissolved. Photostability tests show the evolution of hydrogen upon irradiation even in the dark. It is proposed that hydrogen evolution derives from the deprotonation of the ammonium ligand followed by the decomposition of HI acid. XPS analysis provides evidence in support of this claim, also showing the formation of some Pb^{4+} species on the surface. Overall, the present study illustrates the potential that a proper selection of the organic ligand can have not only with respect to the electronic properties and structure of the hybrid perovskite, but also to perform further modification in the material.

Conflicts of interest

There are no conflicts to declare.

Acknowledgements

Financial support from the Spanish Ministry of Economy and Competitiveness (Severo Ochoa, and RTI2018-9890237-CO2-R1) and the Generalitat Valenciana (Prometeo 2017/083) is gratefully acknowledged. Yong Peng also thanks the Universitat Politecnica de Valencia for a predoctoral scholarship.

Notes and references

1. Lee, M. M.; Teuscher, J.; Miyasaka, T.; Murakami, T. N.; Snaith, H. J., Efficient Hybrid Solar Cells Based on Meso-Superstructured Organometal Halide Perovskites. *Science* **2012,** *338*, 643-647.

2. Boix, P. P.; Agarwala, S.; Koh, T. M.; Mathews, N.; Mhaisalkar, S. G., Perovskite Solar Cells: Beyond Methylammonium Lead Iodide. *The Journal of Physical Chemistry Letters* **2015,** *6*, 898-907.

3. Eames, C.; Frost, J. M.; Barnes, P. R. F.; O'Regan, B. C.; Walsh, A.; Islam, M. S., Ionic transport in hybrid lead iodide perovskite solar cells. *Nature Communications* **2015,** *6*, 7497.

4. Kato, Y.; Ono, L. K.; Lee, M. V.; Wang, S.; Raga, S. R.; Qi, Y., Silver Iodide Formation in Methyl Ammonium Lead Iodide Perovskite Solar Cells with Silver Top Electrodes. *Advanced Materials Interfaces* **2015,** *2*, 1500195.

5. Malinkiewicz, O.; Yella, A.; Lee, Y. H.; Espallargas, G. M.; Graetzel, M.; Nazeeruddin, M. K.; Bolink, H. J., Perovskite solar cells employing organic charge-transport layers. *Nature Photonics* **2013,** *8*, 128.

6. Christians, J. A.; Manser, J. S.; Kamat, P. V., Multifaceted Excited State of CH3NH3PbI3. Charge Separation, Recombination, and Trapping. *The Journal of Physical Chemistry Letters* **2015,** *6*, 2086-2095.

7. Stranks, S. D.; Eperon, G. E.; Grancini, G.; Menelaou, C.; Alcocer, M. J. P.; Leijtens, T.; Herz, L. M.; Petrozza, A.; Snaith, H. J., Electron-Hole Diffusion Lengths Exceeding 1 Micrometer in an Organometal Trihalide Perovskite Absorber. *Science* **2013,** *342*, 341-344.

8. Xing, G.; Mathews, N.; Sun, S.; Lim, S. S.; Lam, Y. M.; Grätzel, M.; Mhaisalkar, S.; Sum, T. C., Long-Range Balanced Electron- and Hole-Transport Lengths in Organic-Inorganic CH3NH3PbI3. *Science* **2013,** *342*, 344-347.

9. Albero, J.; García, H., Luminescence control in hybrid perovskites and their applications. *J. Mater. Chem. C* **2017,** *5*, 4098-4110.

10. Correa-Baena, J.-P.; Abate, A.; Saliba, M.; Tress, W.; Jesper Jacobsson, T.; Grätzel, M.; Hagfeldt, A., The rapid evolution of highly efficient perovskite solar cells. *Energy Environ. Sci.* **2017,** *10*, 710-727.

11. Jeon, N. J.; Na, H.; Jung, E. H.; Yang, T.-Y.; Lee, Y. G.; Kim, G.; Shin, H.-W.; Il Seok, S.; Lee, J.; Seo, J., A fluorene-terminated hole-transporting material for highly efficient and stable perovskite solar cells. *Nature Energy* **2018,** *3*, 682-689.

12. Sahli, F.; Werner, J.; Kamino, B. A.; Bräuninger, M.; Monnard, R.; Paviet-Salomon, B.; Barraud, L.; Ding, L.; Diaz Leon, J. J.; Sacchetto, D.; Cattaneo, G.; Despeisse, M.; Boccard, M.; Nicolay, S.; Jeangros, Q.; Niesen, B.; Ballif, C., Fully textured monolithic perovskite/silicon tandem solar cells with 25.2% power conversion efficiency. *Nature Materials* **2018,** *17* (9), 820-826.

13. Dhakshinamoorthy, A.; Navalon, S.; Corma, A.; Garcia, H., Photocatalytic CO2 reduction by TiO2 and related titanium containing solids. *Energy Environ. Sci.* **2012,** *5*, 9217-9233.

14. Albero, J.; Asiri, A. M.; García, H., Influence of the composition of hybrid perovskites on their performance in solar cells. *J. Mater. Chem. A* **2016,** *4*, 4353-4364.

15. Park, S.; Chang, W. J.; Lee, C. W.; Park, S.; Ahn, H.-Y.; Nam, K. T., Photocatalytic hydrogen generation from hydriodic acid using methylammonium lead iodide in dynamic equilibrium with aqueous solution. *Nature Energy* **2016,** *2*, 16185.

16. Niu, G.; Guo, X.; Wang, L., Review of recent progress in chemical stability of perovskite solar cells. *J. Mater. Chem. A* **2015,** *3*, 8970-8980.

17. Sharma, S. K.; Phadnis, C.; Das, T. K.; Kumar, A.; Kavaipatti, B.; Chowdhury, A.; Yella, A., Reversible Dimensionality Tuning of Hybrid Perovskites with Humidity: Visualization and Application to Stable Solar Cells. *Chemistry of Materials* **2019,** *31*, 3111-3117.

18. Berhe, T. A.; Su, W.-N.; Chen, C.-H.; Pan, C.-J.; Cheng, J.-H.; Chen, H.-M.; Tsai, M.-C.; Chen, L.-Y.; Dubale, A. A.; Hwang, B.-J., Organometal halide perovskite solar cells: degradation and stability. *Energy & Environmental Science* **2016,** *9* (2), 323-356.

19. Wang, R.; Mujahid, M.; Duan, Y.; Wang, Z.-K.; Xue, J.; Yang, Y., A Review of Perovskites Solar Cell Stability. *Advanced Functional Materials 0* (0), 1808843.

20. Ma, J.; Fang, C.; Chen, C.; Jin, L.; Wang, J.; Wang, S.; Tang, J.; Li, D., Chiral 2D Perovskites with a High Degree of Circularly Polarized Photoluminescence. *ACS Nano* **2019,** *13*, 3659-3665.

21. Tremblay, M. H.; Thouin, F.; Leisen, J.; Bacsa, J.; Srimath Kandada, A. R.; Hoffman, J. M.; Kanatzidis, M. G.; Mohite, A. D.; Silva, C.; Barlow, S.; Marder, S. R., (4NPEA)2PbI4 (4NPEA = 4-Nitrophenylethylammonium): Structural, NMR, and Optical Properties of a 3 × 3 Corrugated 2D Hybrid Perovskite. *Journal of the American Chemical Society* **2019,** *141*, 4521-4525.

22. Spanopoulos, I.; Hadar, I.; Ke, W.; Tu, Q.; Chen, M.; Tsai, H.; He, Y.; Shekhawat, G.; Dravid, V. P.; Wasielewski, M. R.; Mohite, A. D.; Stoumpos, C. C.; Kanatzidis, M. G., Uniaxial Expansion of the 2D Ruddlesden-Popper Perovskite Family for Improved Environmental Stability. *Journal of the American Chemical Society* **2019,** *141*, 5518-5534.

23. Febriansyah, B.; Koh, T. M.; John, R. A.; Ganguly, R.; Li, Y.; Bruno, A.; Mhaisalkar, S. G.; England, J., Inducing Panchromatic Absorption and Photoconductivity in Polycrystalline Molecular 1D Lead-Iodide Perovskites through π-Stacked Viologens. *Chemistry of Materials* **2018,** *30*, 5827-5830.

24. Zhao, Y.-Q.; Ma, Q.-R.; Liu, B.; Yu, Z.-L.; Yang, J.; Cai, M.-Q., Layer-dependent transport and optoelectronic property in two-dimensional perovskite: (PEA)2PbI4. *Nanoscale* **2018,** *10*, 8677-8688.

25. Byun, J.; Cho, H.; Wolf, C.; Jang, M.; Sadhanala, A.; Friend, R. H.; Yang, H.; Lee, T.-W., Efficient Visible Quasi-2D Perovskite Light-Emitting Diodes. *Advanced Materials* **2016,** *28*, 7515-7520.

26. Li, N.; Zhu, Z.; Chueh, C.-C.; Liu, H.; Peng, B.; Petrone, A.; Li, X.; Wang, L.; Jen, A. K.-Y., Mixed Cation FAxPEA1–xPbI3 with Enhanced Phase and Ambient Stability toward High-Performance Perovskite Solar Cells. *Advanced Energy Materials* **2017,** *7*, 1601307.

27. Arabpour Roghabadi, F.; Alidaei, M.; Mousavi, S. M.; Ashjari, T.; Tehrani, A. S.; Ahmadi, V.; Sadrameli, S. M., Stability progress of perovskite solar cells dependent on the crystalline structure: From 3D ABX3 to 2D Ruddlesden–Popper perovskite absorbers. *Journal of Materials Chemistry A* **2019,** *7* (11), 5898-5933.

28. Khuong, K. S.; Jones, W. H.; Pryor, W. A.; Houk, K. N., The Mechanism of the Self-Initiated Thermal Polymerization of Styrene. Theoretical Solution of a Classic Problem. *Journal of the American Chemical Society* **2005,** *127* (4), 1265-1277.
29. Yao, K.; Wang, X.; Li, F.; Zhou, L., Mixed perovskite based on methyl-ammonium and polymeric-ammonium for stable and reproducible solar cells. *Chemical Communications* **2015,** *51* (84), 15430-15433.
30. Bubnova, O., 2D materials: Hybrid interfaces. *Nature Nanotechnology* **2016**.
31. Saidaminov, M. I.; Abdelhady, A. L.; Murali, B.; Alarousu, E.; Burlakov, V. M.; Peng, W.; Dursun, I.; Wang, L.; He, Y.; Maculan, G.; Goriely, A.; Wu, T.; Mohammed, O. F.; Bakr, O. M., High-quality bulk hybrid perovskite single crystals within minutes by inverse temperature crystallization. *Nature Communications* **2015,** *6*, 7586.
32. Baikie, T.; Fang, Y.; Kadro, J. M.; Schreyer, M.; Wei, F.; Mhaisalkar, S. G.; Graetzel, M.; White, T. J., Synthesis and crystal chemistry of the hybrid perovskite (CH3NH3)PbI3 for solid-state sensitised solar cell applications. *J. Mater. Chem. A* **2013,** *1*, 5628-5641.
33. Dou, L.; Wong, A. B.; Yu, Y.; Lai, M.; Kornienko, N.; Eaton, S. W.; Fu, A.; Bischak, C. G.; Ma, J.; Ding, T.; Ginsberg, N. S.; Wang, L.-W.; Alivisatos, A. P.; Yang, P., Atomically thin two-dimensional organic-inorganic hybrid perovskites. *Science* **2015,** *349*, 1518-1521.
34. Milot, R. L.; Sutton, R. J.; Eperon, G. E.; Haghighirad, A. A.; Martinez Hardigree, J.; Miranda, L.; Snaith, H. J.; Johnston, M. B.; Herz, L. M., Charge-Carrier Dynamics in 2D Hybrid Metal–Halide Perovskites. *Nano Letters* **2016,** *16*, 7001-7007.
35. Véron, A. C.; Linden, A.; Leclaire, N. A.; Roedern, E.; Hu, S.; Ren, W.; Rentsch, D.; Nüesch, F. A., One-Dimensional Organic–Inorganic Hybrid Perovskite Incorporating Near-Infrared-Absorbing Cyanine Cations. *The Journal of Physical Chemistry Letters* **2018,** *9*, 2438-2442.
36. Peng, Y.; Albero, J.; Álvarez, E.; García, H., Hybrid benzidinium lead iodide perovskites with a 1D structure as photoinduced electron transfer photocatalysts. *Sustainable Energy Fuels* **2019**, -.
37. Wang, S.; Ono, L. K.; Leyden, M. R.; Kato, Y.; Raga, S. R.; Lee, M. V.; Qi, Y., Smooth perovskite thin films and efficient perovskite solar cells prepared by the hybrid deposition method. *J. Mater. Chem. A* **2015,** *3*, 14631-14641.
38. Zhang, F.; Srinivasan, M. P., Multilayered Gold-Nanoparticle/Polyimide Composite Thin Film through Layer-by-Layer Assembly. *Langmuir* **2007,** *23*, 10102-10108.
39. Singh, T.; Öz, S.; Sasinska, A.; Frohnhoven, R.; Mathur, S.; Miyasaka, T., Sulfate-Assisted Interfacial Engineering for High Yield and Efficiency of Triple Cation Perovskite Solar Cells with Alkali-Doped TiO2 Electron-Transporting Layers. *Advanced Functional Materials* **2018,** *28*, 1706287.
40. Yang, J.; Kelly, T. L., Decomposition and Cell Failure Mechanisms in Lead Halide Perovskite Solar Cells. *Inorganic Chemistry* **2017,** *56*, 92-101.
41. Huang, W.; Manser, J. S.; Kamat, P. V.; Ptasinska, S., Evolution of Chemical Composition, Morphology, and Photovoltaic Efficiency of CH3NH3PbI3 Perovskite under Ambient Conditions. *Chemistry of Materials* **2016,** *28*, 303-311.